Volume 1 | Number 1 | Jan 2013 | Pages 1–100

Nanoscale

www.rsc.org/nanoscale

ROYAL SOCIETY OF CHEMISTRY

This is an *Accepted Manuscript*, which has been through the Royal Society of Chemistry peer review process and has been accepted for publication.

Accepted Manuscripts are published online shortly after acceptance, before technical editing, formatting and proof reading. Using this free service, authors can make their results available to the community, in citable form, before we publish the edited article. We will replace this *Accepted Manuscript* with the edited and formatted *Advance Article* as soon as it is available.

You can find more information about *Accepted Manuscripts* in the **Information for Authors**.

Please note that technical editing may introduce minor changes to the text and/or graphics, which may alter content. The journal's standard **Terms & Conditions** and the **Ethical guidelines** still apply. In no event shall the Royal Society of Chemistry be held responsible for any errors or omissions in this *Accepted Manuscript* or any consequences arising from the use of any information it contains.
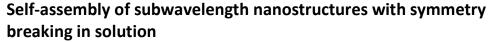
Nanoscale

Self-assembly of subwavelength nanostructures with symmetry breaking in solution

Xiang-Dong Tian,*[a] Shu Chen,[b] Yue-Jiao Zhang,[c] Jin-Chao Dong,[c] Rajapandiyan Panneerselvam,[c] Yun Zhang,*[a] Zhi-Lin Yang,[b] Jian-Feng Li*[c] and Zhong-Qun Tian[c]

Nanostructures with symmetry breaking can allow the coupling between dark and bright plasmon modes to induce strong Fano resonance. However, it is still a daunting challenge to prepare bottom-up self-assembled subwavelength asymmetric nanostructures with appropriate gaps between the nanostructures especially below 5 nm in solution. Here we present a viable self-assembly method to prepare symmetry-breaking nanostructures consisted of Ag nanocubes and Au nanoshperes both with tunable size (90-250 nm for Au nanospheres; 100-160 nm for Ag nanocubes) and meanwhile control the nanogaps through the ultrathin silica shells of 1-5 nm thickness. Raman tag of 4-mercaptobenzoic acid (MBA) assists the self-assembly process and endows the subwavelength asymmetric nanostructures with surafce-enhanced Raman scattering (SERS) activity. Moreover, thick silica shells (above 50 nm thickness) can be coated on the self-assembled nanostructures in situ to stabilize the whole nanostucutres, paving the way toward bioapplications. Single particle scattering spectroscopy with a 360° polarization resolution is performed on individual Ag nanocube and Au nanoshpere dimers, correlated with high-resolution TEM characterization. The asymmetric dimers exhibit strong configuration and polarization dependence Fano resonance property. Overall, the solution-based self-assembly method reported here is opening up new opportunities to prepare diverse multicomponent nanomaterials with optimal performance.

Introduction

Fano resonance is an emerging area of investigation aiming to illuminate the relationship between nanostructures and Fano properties. The sharp plasmon linewidth of the Fano resonance and huge field enhancement at the Fano wavelength point [1-3] attract applications in a wide range of fields such as ultrasensitive chemical and biological sensors,[4, 5] nonlinear and slow-light devices.[6-8] In particular, subwavelength nanostructures with symmetry breaking can produce strong Fano resonance effects due to the improved near-field coupling of bright modes and dark modes.[2, 9-11] Asymmetric nanostructures such as dolmen-type arranged slab structures,[12, 13] non-concentric ring-disk cavity,[14] ring-disk dimer,[13] and metallic nanodisk with a missing wedge-shaped slice[15] can well support Fano resonance. However, all the above mentioned nanostructures are constructed through the top-down route, such as electron-beam lithography, electron-beam evaporation and atomic layer deposition.

[a.] Xiamen Institute of Rare-earth Materials, Chinese Academy of Sciences, Xiamen 361005, China.
Email: tianxd@fjirsm.ac.cn; zhangy@fjirsm.ac.cn;
[b.] Department of Physics, Xiamen University, Xiamen 361005, China.
[c.] State Key Laboratory of Physical Chemistry of Solid Surfaces and Department of Chemistry, College of Chemistry and Chemical Engineering, Xiamen University, Xiamen 361005, China.
Email: li@xmu.edu.cn
† Electronic Supplementary Information (ESI) available: [Materials, experimental details including synthesis, and characterization.]. See DOI: 10.1039/x0xx00000x

Bottom-up self-assembly is an alternative way to prepare complex nanostructures with chemical synthesis nanoparticles as building blocks.[16-18] Nowadays a great many chemical synthesis protocols have been established to prepare various nanoparticles with tunable plasmonics properties through decades of endeavors by the community of nano-researchers worldwide,[19] forming the current building block library. Compared to individual structural units made via the top-down route, the chemical synthesis nanoparticles possess higher optical quality with sharper plasmon linewidth due to the smooth surfaces.[20] More importantly, bottom-up assembly can give access to gaps of nanostructures within 1-5 nm,[21, 22] even down to the subnanometer range,[23-25] which is still a big challenge for top-down approach. In fact, this range of gap dimension enters into one of the physical realms dominated by single-molecule surface enhanced Raman scattering.[26] The assembly of nanoparticles into one-, two-, and three-dimensional well-organized nanostructures have fostered the potential applications in the areas of plasmonic based sensing and detection,[27-29] hot electrons based photovoltaic,[30] highly efficient catalysts,[31] and metamaterials.[32-34] Although much attention has been paid to organize nanoparticle building blocks into complex macroscopic structures through the bottom-up approach.[16, 18, 30-33] Subwavelength asymmetric nanostructures can also be assembled to present special optical properties. Lombardi et al. synthesized Au nanospheres and Ag nanospheres heterodimers with the gaps separated by 16 nm thickness silica shells coated on Au nanospheres. The

extinction spectra of the Au-Ag heterodimers exhibited two resonance peaks attributing to the characteristic plasmonic bands of Au and Ag nanospheres respectively.[35] Biswas and co-workers prepared dolmen type nanostructures through chemically synthesized colloidal gold nanorods, which showed Fano resonance due to the symmetry breaking of the nanostructures.[20] They also synthesized gold nanorod heterodimers through the bottom-up self-assembly method, presenting Fano induced transparency in the visible wavelengths.[36] Recently, Yang et al. prepared gold nanorod dimers with a longitudinal offset through feedback-driven self-assembly.[37] The symmetry-breaking dimers can give rise to magnetic dipolar resonance.

Mismatched with the high-volume nanoparticle library available, the building blocks used for the assembly of subwavelength asymmetric nanostructures are mainly Au nanorods, Au nanospheres and Ag nanospheres as showed above. However, it will be a significant breakthrough in the assembly of subwavelength asymmetric nanostructures if these requirements are met: (1) the assembled unit can be consisted of nanoparticles with different shapes and components. (2) The size of each building block within the assembly unit should be tuned separately over a wide range (10 -200 nm). (3) The gaps between touched nanoparticles within the unit should be tuned from around 1 nm to beyond 10 nm. (4) The production of a certain type nanostructure with high yield should be scalable. (5) The assembled nanostructures can be stabilized in solution by postprocessing. (6) It is important to reveal the relationships between the asymmetric nanostructures and the optical properties, assisting in the rational design of nanostructures. (7) The subwavelength asymmetric nanostructures can be further assembled into macroscopic structures for practical applications.

With these thoughts in mind, here we develop a solution–based self-assembly strategy that allows for creating a series of subwavelength asymmetric nanostructures (Fig. 1). Two types of building blocks, Au nanospheres with diameters from 90 to 250 nm, Ag nanocubes with edges from 100 to 160 nm, are utilized to assemble the Au nanosphere and Ag nanocube subwavelength nanostructures with symmetry breaking, then coated with thick silica shells to stabilizing the whole nanostructures (denoted as (Au-Ag)@SiO$_2$ for dimers, (Ag-Au-Ag)@SiO$_2$ for trimers). The gaps between touched nanoparticles within an assembly unit is controlled by the thickness of ultrathin silica shells from 1 to above 10 nm. Single particle scattering spectroscopy is then used to disclose the relationship between the structure and plasmonic property through the correlated transmission electron microscope (TEM) characterization and the 360° polarization-resolved scattering study. Pronounced Fano resonances appear when the polarization direction normal to the dimer axis. The bottom-up self-assembly strategy developed here sheds some light not only on the design of novel plasmonic materials, but even more important on integrating the plasmonic units with the photocatalytic units to form functional nanostructures.
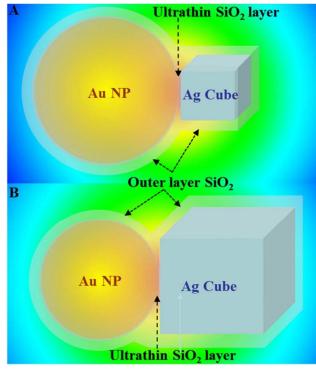

Fig. 1 Schematic illustration of the self-assembly of the asymmetric nanostructures with adjustable building blocks (A and B) in solution. The gap is controlled by ultrathin silica shells. The whole nanostructures are stabilized by thick silica shells.

Results and discussion

Synthesis of the building blocks

Au nanospheres with diameters up to 250 nm were synthesized through a seeded growth approach.[38] This way can produce uniform spherical shape Au nanoparticles with narrow size distributions, and that with sodium citrate as ligands (Fig. S1 and S2 in Supporting Information). Ag nanocubes were synthesized through a two-channel injection method with 1, 5-pentanediol as the solvent and reducer.[25, 39] The size of the Ag nanocubes can be tuned from 100 to 160 nm by quenching the reaction at different time points (Fig. S3 in Supporting Information). Au nanospheres and Ag nanocubes are the two building blocks for the following self-assembly of asymmetric nanostructures.

The coating of Au nanospheres with ultrathin silica shells

To control the gaps between Au and Ag nanoparticles, ultrathin silica shells with adjustable thicknesses of 1-5 nm were coated on the surface of Au nanospheres. The ultrathin silica shells can isolate the exchange of free electrons to increase the quality of plasmonics, based on which a powerful surface analysis method have been developed and named as shell-isolated nanoparticle-enhanced Raman spectroscopy (SHINERS).[40] In this work, 4-mercaptobenzoic acid (MBA) was used to make the Au nanosphere surfaces amenable to the growth of the ultrathin silica shells,[41] instead of (3-

aminopropyl)-trimethoxysilane (APTES) used in the previous reports.[42] However, it is interested that the growth of silica shell is much slower when MBA is used
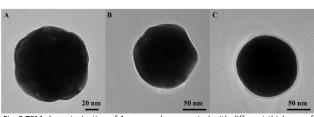

Fig. 2 TEM characterization of Au nanospheres coated with different thickness of silica shells. The thickness of the silica shells of (A) 1.6 nm, (B) 2.8 nm, and (C) 5.0 nm. (A) With MBA as the primer, (B) and (C) with APTES as the primer.

as the primer and sodium silicate as Si source, compared to the APTES cases, thereby potentially providing a preferable way to coat Au nanospheres with the thickness of silica shells below 2 nm. Here APTES was used to synthesize silica shells beyond 2 nm and up to a thickness of 10 nm. Fig. 2 shows the ultrathin silica shells synthesized around 120 nm Au nanospheres through the two ways: the thickness of silica shells of (A) is ~2 nm through MBA as the primer, (B) ~3 nm and (C) ~5 nm are by the APTES way. The ultrathin silica shells could direct the assembly with Ag nanocubes through the surfaces modified with thiol or amine groups.

The assembly of Au-Ag asymmetric nanostructures with adjustable building block sizes

The driving forces for the assembly between Au and Ag nanoparticles are mainly due to the high affinity of thiols or amines binding to the Ag surface. As discussed above, the growth of silica shells on Au cores was quite slow when MBA was used as the primer for the formation of silica layers. One possible reason is that the carboxyl group of MBA can anchor it on the silica surface, making the thiol pointed into solution. It was deduced that MBA can greatly reduce the growth of silica shells by decreasing the number of silanol groups exposed for the hydrolytic condensation. However the exposed thiol groups on silica shells can be utilized to direct the self-assembly of Au nanospheres with Ag nanocubes, meanwhile separating the nanoparticles by the thickness of silica shells. Based on this finding, subwavelength asymmetric nanostructures consisted of Au nanospheres and Ag nanocubes with different sizes were prepared. Au nanospheres of different sizes were first functionalized with ~1 nm thickness silica shells terminated with SH groups. Subsequently, these nanoparticles were self-assembled with different size Ag nanocubes in solution to produce a series of asymmetric nanostructures. Fig. 3 shows the representative nanostructures. Fig. 3 (A) and (B) show the asymmetric nanostructures consisted of Au nanospheres with diameter 125 nm and Ag nanocubes with edge length 100 nm. Au nanospheres with diameters above 200 nm can well assemble with Ag nanocubes of 100 nm, as shown in Fig. 3(C) and (D). It can be seen from Fig. 3(C) that besides Au-Ag dimers, quite a number of Ag-Au-Ag trimers were also produced due to the

much larger size of Au nanospheres than Ag nanocubes, offering rich attaching sites. The edge length of Ag nanocubes can also be changed with the self-assembled nanostructures. Fig. 3(E) and (F) show asymmetric nanostructures including Ag nanocubes with dimensions bigger than the Au nanospheres. It should be noted that the gaps within the assembled nanostructures for all the samples shown in Fig. 3 were kept around 1 nm through the ultrathin silica shells that had been already coated on Au nanospheres (Fig. S4).

The subwavelength asymmetric nanostructures Au-Ag dimers and Au-(Ag)$_2$ trimers are counted together to assess the assembly yield. The yield of the dimers and trimers with 125 nm Au nanospheres and 100 nm Ag nanocubes as building blocks (Fig. 3(A) and (B)) can reach 38% among 300 particles (including monomers and multimers>3). The efficiency of the self-assembly between 220 nm Au nanospheres and 100 nm Ag nanocubes can reach 41% among 300 particles (monomers and multimers>3). However, the self-assembly efficiency of 120 nm Au nanospheres with 140 nm Ag nanocubes decreased to 35% due to the much larger volume of Ag nanocubes than Au nanospheres (~3 times). The much larger size of Ag nanocubes can result in steric hindrance in the Au-Ag dimer to a point where it could not accommodate one more Ag nanocube, reducing the efficiency to form the Ag-Au-Ag trimers. The assembly yields for all types of dimers and trimmers are listed in the table S1. It should be well noted that the Au-Ag dimers and Ag-Au-Ag trimers for all the samples can be further purified from monomers by the routine use of centrifugation.

The assembly of Au-Ag asymmetric nanostructures with tunable gap distances

We also synthesized Au nanospheres and Ag nanocubes asymmetric nanostructures with larger gaps of above 2 nm. Gap distances of the assembled nanostructures around 2 nm can be achieved by using MBA as the primer and extended growth time, as shown in Fig. 4(A). Silica shells with thickness from 4 nm to 10 nm were coated on the Au nanosphere surface through the use of APTES as the primer. Further the silica shells were modified with APTES to endow the surface with exposed amine groups. The strong chemical interactions between Ag and primary amines initiated the self- assembly of Au nanospheres and Ag nanocubes. Here we used Au nanospheres with diameter of 120 nm and Ag nanocubes with edge of 100 nm as the building blocks for the self-assembly, as shown in Fig. 4. The gaps of the nanostructures are shown in Fig. 4 (B) is ~4 nm and ~8 nm in Fig. 4(C). To prepare silica shells thicker than 50 nm, we transferred the Au nanospheres coated with 8 nm silica shells to the TEOS system for the further growth to about 50 nm thickness. After treating the silica surface with APTES, they also could well assemble with Ag nanocubes, as shown in Fig. 4(D).

Analysis of the populations of the assembly nanostructures

For the asymmetric nanostructures with silica gaps around 1 nm, the assembly is directed by the strong interaction between Ag nanocubes and thiol groups anchored on the

ARTICLE   **Nanoscale**

Au@SiO$_2$ nanospheres, forming the Au-S covalent bonds. The assembly reactions can be expressed as:

Au@SiO$_2$+Ag → Au@SiO$_2$-Ag (Au-Ag for short) (1)

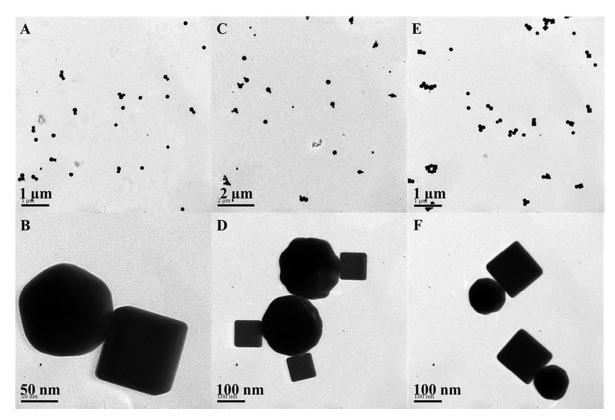Au@SiO$_2$-Ag+Ag → Ag-Au@SiO$_2$-Ag (Au-(Ag)$_2$ for short) (2)

Fig. 3 TEM characterization of the asymmetric nanostructures consisted of Au nanospheres and Ag nanocubes with gaps around 1 nm. (A), (B) The diameter of the Au nanospheres is about 125 nm, the edge length of the Ag nanocubes is about 100 nm. (C), (D) Au nanospheres: 220 nm, Ag nanocubes: 100 nm. (E), (F) Au nanospheres: 120 nm, Ag nanocubes: 140 nm
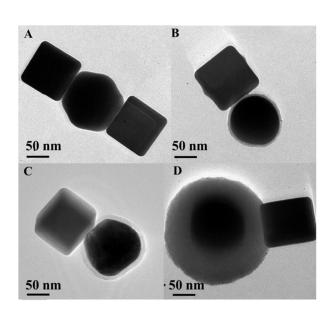

Fig. 4. TEM characterization of the asymmetric nanostructures consisted of Au nanospheres and Ag nanocubes with adjustable gap distances. Gaps between touched nanoparticles are controlled by the thickness of silica shells (A) gap: 2.0 nm, (B) gap: 4.1 nm, (C) gap: 8.3 nm, (D) gap: 50 nm. All the samples were synthesized with 120 nm Au nanospheres and 100 nm Ag nanocubes as the building blocks.

From the chemical reaction view,[43] the assembly efficiency is controlled by the concentrations of Au@SiO$_2$ nanospheres and Ag nanocubes, the coverage degree of thiol groups on Au@SiO$_2$ surfaces and the assembly temperature. Due to the excess amount of MBA (five monolayers of MBA amount), the coverage degree of the thiol groups can be assumed to be full monolayer (100%) or a fixed maximum value, beneficial to highest assembly efficiency. The assembly is proceeded at room temperature. The concentrations of Au@SiO$_2$ nanospheres and Ag nanocubes for the assembly reactions are listed in table 1.

The concentrations of the nanoparticles are the major factors to control the available Ag nanocubes for each Au@SiO$_2$ nanosphere to collide. The concentrations of the 90, 120 and 220 nm Au@SiO$_2$ nanospheres are determined to keep the total surface area of the nanoparticles constant, as

shown in table 1. The concentration of 100 nm Ag nanocubes is 170 pM across all the assembly systems. The concentration ratios of Ag nanocubes with respect to Au@SiO$_2$ nanospheres determine the available maximum coordination numbers as shown in table 1. It can be expected that the most possible assembly nanostructures are Au-Ag dimers for the 120 nm

Au@SiO$_2$ nanospheres. It has been confirmed by the highest assembly yield of dimers achieved among the whole assembly products (30%, table S1 and Fig. 3(A)). For the 90 nm Au@SiO$_2$, the rate of the concentrations is reduced to 0.57, decreasing the
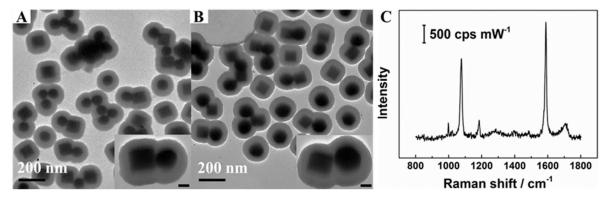

Fig. 5 TEM characterization of the asymmetric nanostructures consisted of Au nanospheres and Ag nanocubes coated with thick silica shells. (A) 90 nm Au nanospheres assembled with 100 nm Ag nanocubes; (B) 120 nm Au nanospheres assembled with 100 nm Ag nanocubes; for both cases the thickness of the silica shells are more than 50 nm. (C) SERS spectrum of MBA obtained through the aqueous suspensions of the asymmetric nanostructures of (B). The inset scale bars are 20 nm.

assembly yield of the dimer to 21%. The yield of Au-(Ag)$_2$ trimers is nearly negligible (1%). However a few linear Au-Ag-Au (Au-(Ag)$_{0.5}$) trimers were produced due to the excess amount of 90 nm Au@SiO$_2$ nanospheres. It should be noted that the assembly nanostructures of Au-(Ag)$_n$ only with n equal or bigger than 1 are considered. For the 220 nm Au@SiO$_2$ and 100 nm Ag nanocubes assembly system, the concentration ratio limits the maximum coordination number of n to 3.4. The assembly yield of the dimer is 24%, slightly lower than that of 120 nm Au@SiO$_2$ case (30%). Nonetheless, the assembly yield of Au-(Ag)$_2$ is improved to 17%, highest among all the assembly systems.

During the formation of Au-(Ag)$_2$ trimers, expressed with equation 2, the approaching of one more Ag nanocubes onto the Au-Ag dimer will arise extra repulsive forces such as steric hindrance and charge repulsion among Ag nanocubes. Due to that the Ag nanocubes are protected by PVP, a well-known neutral surfactant, thus, the only repulsive force is the steric hindrance effect among the Ag nanocubes. The maximum coordination numbers for 100 nm Ag nanocubes packing closely on the Au nanospheres can be calculated as shown in table1. It is evident from table 1 that the coordination numbers determined by the concentration ratios are far below the theoretical limit of the close packing accordingly. The steric hindrance effect should not be prominent in the assembly conditions here. Thus there are spaces to synthesize Au-(Ag)$_3$ tetramers or Au-(Ag)$_4$ pentamers as main products for the 120 and 220 nm Au@SiO$_2$ systems if higher excess of Ag nanocubes are used.

Although the concentration factors have not been well optimized for specific nanostructures, the yield of the dimers and trimers still can be comparable to the published data. Wang and co-authors have synthesized Au nanospheres dimer and trimer nanostructures by directing the assembly of Au nanospheres (18 nm) modified with thiol groups (denoted as A) and Au nanospheres (18 nm or 36 nm) protected by citrate sodium(denoted as B).[43] The concentration of B is 16 times that of A, larger than the close packing number of 12. The yield of dimers and trimers, calculated based on the number of A, can be optimized to about 90% respectively by adjusting the ionic strength of the solution. However if the yield of dimers and trimers is calculated based on the total number of A and B, it will be no more than 10%. Gschneidtner et al. have synthesized heterodimer consisted of a palladium nanocube (25 nm) and an Au nanosphere (90 nm) through the electrostatic interaction of the oppositely charged assembly units, with the optimized yield of 43%.[44] However the yield of the Pd-Au dimers can be lower than 20% when the Pd nanocube concentration is beyond the optimized concentration range. It should be pointed out that due to the large excess (>10 times) of Pd nanocubes used for the assembly reactions, free Pd nanocubes after the assembly are also not counted in for the yield calculations.

The assembly yields in our system are evaluated based on the analysis of the distributions of all types nanostructures after the assembly, including the both free assembly units, Au-Ag

Table 1 The concentrations of Au@SiO₂ nanospheres and Ag nanocubes for the assembly of the nanostructures and the analysis of the possibility of the nanostructure composites

The assembly nanostructures	Au@SiO₂ nanosphere-(Ag nanocube)ₙ denoted as Au-(Ag)ₙ					
	Nanostructure 1		Nanostructure 2		Nanostructure 3	
The assembly units	90 nm Au@SiO₂	100 nm Ag	120 nm Au@SiO₂	100 nm Ag	220 nm Au@SiO₂	100 nm Ag
Concentration/10² (pM)	3.0	1.7	1.7	1.7	0.50	1.7
Maximum coordination number n of Au-(Ag)ₙ under concentration control	0.57		1.0		3.4	
Maximum coordination number n of Au-(Ag)ₙ under steric control	3.0		6.0		15	

dimers, Au-(Ag)$_2$ trimers and the Au-(Ag)$_n$(n>2) multimers, due to the relative low dosage of Ag nanocubes used (see the concentration ratios listed in table 1). The assembly yield reported here will be slightly improved if the number of free Ag nanocubes is removed from the calculations. The purification of the desired nanostructures from the assembly products at yields of above 90% can resort to a powerful separation protocol of differential centrifugation. It has been demonstrated to purify the assembly dimers in high purity (above 90%).[45]

Stabilizing Au-Ag asymmetric nanostructures with thick silica shells

To stabilize the asymmetric nanostructures formed in solution and avoid the direct interaction with the substrate during the sample preparation process, more than 50 nm thickness silica shells were coated on the nanostructures through the TEOS approach.[46, 47] Fig. 5(A), (B) and insets show the Au-Ag dimers, trimers, assembled through 100 nm Ag nanocubes with 90 (A) and 120 (B) nm Au nanospheres respectively, are coated with thick silica shells. The gaps within the nanostructures are around 1 nm as shown in the insets of Fig. 5(A) and (B). It is well known that MBA is a classic SERS tag due to the large Raman scattering cross-section and its strong adsorption interaction with Au and Ag. Therefore the asymmetric nanostructures with MBA as the primer for silica growth can give rise to strong SERS signals due to the small gaps, as shown in Fig. 5(C). The bands at 1076 and 1589 cm-1 are attributed to the aromatic ring vibration of MBA. Additionally, silica coating makes the nanomaterial inert in biological systems and facile for surface functionalization, paving the way for a wide range of biomedical applications.

Plasmonic property of the single (Au-Ag)@SiO₂ and (Ag-Au-Ag)@SiO₂

Due to the recent predicament of assembling unique asymmetric nanostructures with high yields (above 80%), we studied the plasmonics property of the asymmetric nanostructures through single-particle spectroscopy correlated with TEM characterization. Here individual dimers of (Au-Ag)@SiO₂ and trimers of (Ag-Au-Ag)@SiO₂ with Au nanospheres 120 nm and Ag nanocubes 100 nm were investigated. The interparticle gaps were controlled by the ultrathin silica shells of 1 nm thickness. The true colour dark-filed image of the sample is shown in Fig. 6(A) that was taken by a smartphone, as that done in the previous paper. Fig. 6(B)
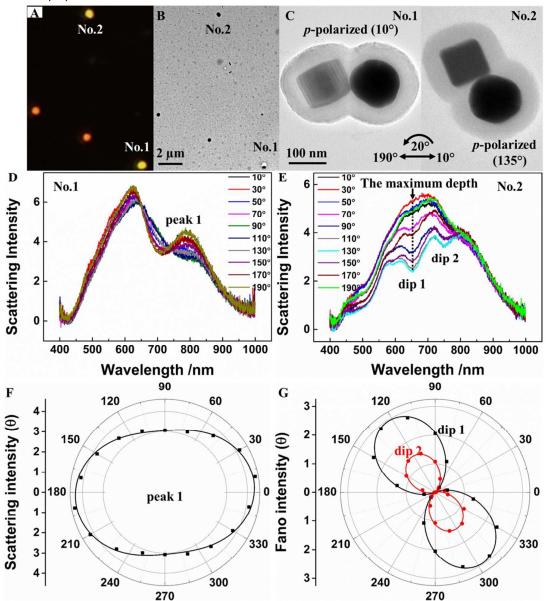
is the correlated TEM characterization. So it is already known that the green-yellow scattering spots were produced by the (Au-Ag)@SiO₂ dimers labelled as No.1 and No.2 respectively in Fig. 6(A) and (B). The remaining two orange-red spots originated from the scattering interaction of 120 nm Au nanospheres with light. Fig. 6(C) is the high resolution TEM image of the No.1 and 2 dimers. The configuration of the No.1 asymmetric nanostructures is the Ag nanocube arranged with the Au nanosphere through the vertex. The centres of the Au nanosphere and the Ag nanocube seem not within the same horizontal plane according to the TEM image. The two nanoparticles in the No.2 dimer align with each other through the face of the nanocube. The attaching point between the two nanoparticles is apart from the centre of the Ag nanocube face.

To understand the plasmonic property of the asymmetric nanostructures, we performed a 360° polarization-dependent scattering study on the No.1 and No.2 dimers, shown in Fig. 6(D) and (E), respectively. The scattering spectroscopy of No.1 dimer shows two peaks, located at 600 nm and 800 nm. The peak at 800 nm changes with the polarization directions including the intensity and wavelength. The peak is gradually insignificant when the polarization direction is changed from parallel to the dimer axis to perpendicular to the dimer axis. The relationship of the peak intensity with the polarization directions is showed in Fig. 6(F). It can be seen that the maximum scattering is parallel to the dimer axis, when overlaying Fig. 6(F) on Fig. 6(C) of the No.1 dimer.

The scattering spectrum of No.2 dimer shows in Fig. 6(E), from which it seems that one broad peak splits into three separate peaks, separated by two dips labelled as 1 and 2. Here the depth of the dip is defined as the distance between each curve and the reference curve (the red curve shown in Fig. 6(E) with the strongest scattering intensity) at the dip wavelength point. The maximum dip depth is measured with the dash line as an example is shown in Fig. 6(E). The relationships of the dip depth with the polarization directions for dip 1 and 2 are shown in Fig. 6(G). It is clearly shown that the largest depth is reached when the polarization direction is parallel to the dimer axis for both the dip 1 and 2 cases if Fig. 6(G) is overlaid above Fig. 6(C) of the No.2 dimer. Another (Au-Ag)@SiO₂ dimer and a (Au-Ag-Au)@SiO₂ trimer present similar spectral responses as shown in Fig. S5 and S6.

To find out the origin of the plasmon modes of the asymmetric nanostructures (No.1 and 2 dimers), we have calculated the scattering spectra and electric field distributions with the FDTD simulations based on the experiment models. The electromagnetic wave illustrates the dimer with polarization parallel and perpendicular to the interparticle axis of the cube-sphere dimer. According to our calculation results of No.1 and No.2, as shown in Fig.7, the lineshapes and changing tendency with the variations of the polarization direction are nearly matched with the experimental scattering spectra. From the simulated results of the No.1 dimer (Fig. 7A), one plasmon mode is excited in the scattering spectra when the polarization is perpendicular to the dimer axis. The broad

scattering peak can be assigned to the uncoupled dipole mode, as further confirmed by the small field enhancement effect at the nanogap of the No.1 dimer, shown in 1 of Fig.7B. The multiple modes are excited with the polarization parallel to the dimer axis (Fig.7A black curve). The typical dipole-dipole coupling mode is located at 890 nm. The two modes marked as 2 and 3 in the visible region can originate from the higher coupling modes of the cube coupling mode. The much higher field enhancements at the hot spot of the No.1 dimer showed in Fig.7B (2 and 3) further display the dimer is on a strong coupling state when the polarization is along the dimer axis. The deviations between experimental and

Fig. 6 Single-particle scattering spectroscopy of individual (Au-Ag)@SiO$_2$ dimers correlated with high-resolution TEM characterization. (A) A dark-field image of the self-assembled (Au-Ag)@SiO$_2$ dimers. (B) The correlated TEM image. (C) High-resolution TEM characterization of the scattering spots labelled as No.1 and No.2 in (A). The polarization direction of the incident light are showed using the arrow and rotated anticlockwise with increment of 20°. (D) Polarization-dependent scattering spectra of the No.1 dimer. (E) Polarization-

dependent scattering spectra of the No.2 dimer. (F) The relationship of the scattering intensity of peak 1 of the No.1 dimer with the polarization angle. (G) The relationship of the Fano intensity of dip 1 and 2 with the polarization angle.

calculated scattering spectra may stem from the uncertainty degrees of cube, the detailed arrangement configuration of the sphere-cube system and the uncertainty of polarized degrees.

Similar to the spectral responses of the No.1 dimer, the uncoupled dipole mode of the No.2 dimer is excited when the polarization is perpendicular to the dimer axis. For the polarization parallel to the dimer axis, the plasmon modes of the face-face contacting cube-sphere system (No.2) is more complex comparing with the vertex contacting situation in cube-sphere systems (No.1), as shown in Fig. 6E and Fig.S7. The asymmetry Fano lineshapes are presented in the 600-800 nm wavelength range and are benefited from the overlapping of the multiple modes.
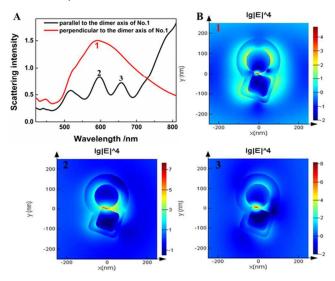

Fig.7 The simulation results of the No.1 dimer. (A) The scattering spectra of the No.1 dimer when electric polarization parallel (black curve) and perpendicular (red curve) to the dimer axis; (B) Electric field distributions of the dimer at peak 1, 2 and 3 respectively.

Conclusions

In conclusion, we have reported a solution-based self-assembly route to prepare subwavelength nanostructures with symmetry breaking. The subwavelength asymmetric nanostructures are consisted of Au nanospheres (diameter: 90-250 nm) and Ag nanocubes (edge: 100-160 nm). Notably, we have shown that the gaps between the touched nanoparticles can be controlled by the ultrathin silica shells (1-5 nm) coated on the Au nanospheres. Raman tag of MBA has been inserted into the subwavelength asymmetric nanostructures, giving rise to a new class of SERS probes. Moreover, further coating of thick silica shells around the whole nanostructures makes the self-assembled nanostructures stable and amenable to the surface functionalization. The correlation of the single-particle scattering spectroscopy and high-resolution TEM image reveals that the Fano resonance response is dependent on the polarization direction and delicate configuration of the nanostructures. In sum, our results attest the feasibility to prepare a new class of metamaterials with tailored optical properties in solution by using plasmonic nanoparticles with diverse components, shapes and dimensions as building blocks.

Notes and references

1. N. J. Halas, S. Lal, W. S. Chang, S. Link and P. Nordlander, *Chem. Rev.*, 2011, **111**, 3913-3961.
2. B. Luk'yanchuk, N. I. Zheludev, S. A. Maier, N. J. Halas, P. Nordlander, H. Giessen and C. T. Chong, *Nat. Mater.*, 2010, **9**, 707-715.
3. J. Q. Wang, X. M. Liu, L. Li, J. N. He, C. Z. Fan, Y. Z. Tian, P. Ding, D. X. Chen, Q. Z. Xue and E. J. Liang, *Journal of Optics*, 2013, **15**.
4. C. Wu, A. B. Khanikaev, R. Adato, N. Arju, A. A. Yanik, H. Altug and G. Shvets, *Nat. Mater.*, 2012, **11**, 69-75.
5. G. Chen, Y. Zhao, G. Fu, P. N. Duchesne, L. Gu, Y. Zheng, X. Weng, M. Chen, P. Zhang, C. W. Pao, J. F. Lee and N. Zheng, *Science*, 2014, **344**, 495-499.
6. L. V. Hau, S. E. Harris, Z. Dutton and C. H. Behroozi, *Nature*, 1999, **397**, 594-598.
7. D. Budker, D. Kimball, S. Rochester and V. Yashchuk, *Phys. Rev. Lett.*, 1999, **83**, 1767.
8. C. Liu, Z. Dutton, C. H. Behroozi and L. V. Hau, *Nature*, 2001, **409**, 490-493.
9. F. Monticone and A. Alù, *J. Mater. Chem. C.*, 2014, **2**, 9059-9072.
10. M. Rahmani, B. Luk'yanchuk and M. H. Hong, *Laser Photonics Rev.*, 2013, **7**, 329-349.
11. Z.-J. Yang, Z.-H. Hao, H.-Q. Lin and Q.-Q. Wang, *Nanoscale*, 2014, **6**, 4985-4997.
12. S. Zhang, D. A. Genov, Y. Wang, M. Liu and X. Zhang, *Phys. Rev. Lett.*, 2008, **101**, 047401.
13. N. Verellen, Y. Sonnefraud, H. Sobhani, F. Hao, V. V. Moshchalkov, P. V. Dorpe, P. Nordlander and S. A. Maier, *Nano Lett.*, 2009, **9**, 1663-1667.
14. F. Hao, P. Nordlander, Y. Sonnefraud, P. V. Dorpe and S. A. Maier, *Acs Nano*, 2009, **3**, 643-652.
15. Z. Fang, J. Cai, Z. Yan, P. Nordlander, N. J. Halas and X. Zhu, *Nano Lett.*, 2011, **11**, 4475-4479.
16. R. J. Macfarlane, M. N. O'Brien, S. H. Petrosko and C. A. Mirkin, *Angew. Chem. Int. Ed.*, 2013, **52**, 5688-5698.

17. M. B. Ross, J. C. Ku, V. M. Vaccarezza, G. C. Schatz and C. A. Mirkin, *Nat. Nanotech.*, 2015, **10**, 453-458.

18. F. Lu, K. G. Yager, Y. Zhang, H. Xin and O. Gang, *Nat. Commun.*, 2015, **6**, 6912.

19. Y. Xia, *Angew. Chem. Int. Ed.*, 2014, **53**, 12268-12271.

20. S. Biswas, J. S. Duan, D. Nepal, R. Pachter and R. Vaia, *Nano Lett.*, 2013, **13**, 2220-2225.

21. X. D. Tian, B. J. Liu, J. F. Li, Z. L. Yang, B. Ren and Z. Q. Tian, *J. Raman Spectrosc.*, 2013, **44**, 994-998.

22. C. Hanske, M. Tebbe, C. Kuttner, V. Bieber, V. V. Tsukruk, M. Chanana, T. A. König and A. Fery, *Nano Lett.*, 2014, **14**, 6863-6871.

23. S. F. Tan, L. Wu, J. K. Yang, P. Bai, M. Bosman and C. A. Nijhuis, *Science*, 2014, **343**, 1496-1499.

24. H. Cha, J. H. Yoon and S. Yoon, *Acs Nano*, 2014, **8**, 8554-8563.

25. X. Tian, Y. Zhou, S. Thota, S. Zou and J. Zhao, *J. Phys. Chem. C*, 2014, **118**, 13801-13808.

26. E. C. Le Ru and P. G. Etchegoin, *Annu. Rev. Phys. Chem.*, 2012, **63**, 65-87.

27. S. Biswas, X. Liu, J. W. Jarrett, D. Brown, V. Pustovit, A. Urbas, K. L. Knappenberger Jr, P. F. Nealey and R. A. Vaia, *Nano Lett.*, 2015, **15**, 1836-1842.

28. A. Martin, C. Schopf, A. Pescaglini, J. J. Wang and D. Iacopino, *Langmuir*, 2014, **30**, 10206-10212.

29. M. Tebbe, M. Mayer, B. A. Glatz, C. Hanske, P. T. Probst, M. B. Müller, M. Karg, M. Chanana, T. A. König and C. Kuttner, *Faraday Discuss.*, 2015, **181**, 243-260.

30. H.-X. Lin, L. Chen, D.-Y. Liu, Z.-C. Lei, Y. Wang, X.-S. Zheng, B. Ren, Z.-X. Xie, G. D. Stucky and Z.-Q. Tian, *J. Am. Chem. Soc.*, 2015, **137**, 2828-2831.

31. E. Auyeung, W. Morris, J. E. Mondloch, J. T. Hupp, O. K. Farha and C. A. Mirkin, *J. Am. Chem. Soc.*, 2015, **137**, 1658-1662.

32. Y. H. Lee, W. Shi, H. K. Lee, R. Jiang, I. Y. Phang, Y. Cui, L. Isa, Y. Yang, J. Wang and S. Li, *Nat. Commun.*, 2015, **6**, 6990.

33. M. J. Rozin, D. A. Rosen, T. J. Dill and A. R. Tao, *Nat. Commun.*, 2015, **6**, 7325.

34. D. J. Park, C. Zhang, J. C. Ku, Y. Zhou, G. C. Schatz and C. A. Mirkin, *Proc. Natl. Acad. Sci.*, 2015, **112**, 977-981.

35. A. Lombardi, M. P. Grzelczak, A. Crut, P. Maioli, I. Pastoriza-Santos, L. M. Liz-Marzán, N. Del Fatti and F. Vallée, *Acs Nano*, 2013, **7**, 2522-2531.

36. S. Biswas, J. S. Duan, D. Nepal, K. Park, R. Pachter and R. A. Vaia, *Nano Lett.*, 2013, **13**, 6287-6291.

37. S. Yang, X. Ni, X. Yin, B. Kante, P. Zhang, J. Zhu, Y. Wang and X. Zhang, *Nat. nanotech.*, 2014, **9**, 1002-1006.

38. C. Ziegler and A. Eychmuller, *J. Phys. Chem. C*, 2011, **115**, 4502-4506.

39. A. Tao, P. Sinsermsuksakul and P. Yang, *Angew. Chem. Int. Ed.*, 2006, **45**, 4597-4601.

40. J. F. Li, Y. F. Huang, Y. Ding, Z. L. Yang, S. B. Li, X. S. Zhou, F. R. Fan, W. Zhang, Z. Y. Zhou and B. Ren, *Nature*, 2010, **464**, 392-395.

41. Y. J. Wong, L. Zhu, W. S. Teo, Y. W. Tan, Y. Yang, C. Wang and H. Chen, *J. Am. Chem. Soc.*, 2011, **133**, 11422-11425.

42. J. F. Li, X. D. Tian, S. B. Li, J. R. Anema, Z. L. Yang, Y. Ding, Y. F. Wu, Y. M. Zeng, Q. Z. Chen and B. Ren, *Nat. Protoc.*, 2013, **8**, 52-65.

43. Y. Wang, G. Chen, M. X. Yang, G. Silber, S. X. Xing, L. H. Tan, F. Wang, Y. H. Feng, X. G. Liu, S. Z. Li and H. Y. Chen, *Nat Commun.*, 2010, **1**, 87.

44. T. A. Gschneidtner, Y. A. D. Fernandez, S. Syrenova, F. Westerlund, C. Langhammer and K. Moth-Poulsen, *Langmuir*, 2014, **30**, 3041-3050.

45. G. Chen, Y. Wang, L. H. Tan, M. X. Yang, L. S. Tan, Y. Chen and H. Y. Chen, *J. Am. Chem. Soc.*, 2009, **131**, 4218-4219.

46. C. Graf, D. L. Vossen, A. Imhof and A. van Blaaderen, *Langmuir*, 2003, **19**, 6693-6700.

47. J. A. Sioss, R. L. Stoermer, M. Y. Sha and C. D. Keating, *Langmuir*, 2007, **23**, 11334-11341.

Nanoscale Accepted Manuscript